



# Efficient and versatile CuNi alloy nanocatalysts for the highly selective hydrogenation of furfural

Jun Wu <sup>a,b</sup>, Guang Gao <sup>a</sup>, Jinlei Li <sup>a,b</sup>, Peng Sun <sup>a</sup>, Xiangdong Long <sup>a,b</sup>, Fuwei Li <sup>a,\*</sup>

<sup>a</sup> State Key Laboratory for Oxo Synthesis and Selective Oxidation, Lanzhou Institute of Chemical Physics, Chinese Academy of Sciences, Lanzhou 730000, PR China

<sup>b</sup> University of Chinese Academy of Sciences, Beijing 100039, PR China



## ARTICLE INFO

### Article history:

Received 30 June 2016

Received in revised form

20 September 2016

Accepted 14 October 2016

Available online 15 October 2016

### Keywords:

CuNi alloy

Layered double hydroxides

Selective hydrogenation

Furfural

Highly dispersed

## ABSTRACT

The development of efficient and environmental benign non-noble bimetallic nanocatalysts is highly desirable and attractive in the upgrading of biomass-derived platform compounds to high-valued chemicals. A series of highly dispersed and versatile  $\text{Cu}_x\text{Ni}_y$  ( $x/y = 7:1, 3:1, 1:1, 1:3, 1:7$ ) alloy supported nanocatalysts derived from layer double hydroxides (LDHs) precursors were fabricated and used for the selective hydrogenation of furfural to tetrahydrofurfuryl alcohol (THFA) and furfuryl alcohol (FOL). It was found that the chemical composition, preparation method and especially the reduction temperature of LDHs precursors greatly affected the properties of the resultant  $\text{Cu}_x\text{Ni}_y/\text{MgAlO}$  catalysts. Systematic characterizations revealed that the reduction temperature of catalyst precursor was closely related to the dispersion and homogeneous composition of CuNi alloy nanoparticle as well as the surface basicity of catalysts, which played crucial roles in achieving excellent catalytic performances. The optimized  $\text{CuNi}/\text{MgAlO}$  and  $\text{Cu}_1\text{Ni}_3/\text{MgAlO}$  nanocatalysts showed high activity and selectivity for the hydrogenation of furfural to THFA in ethanol compared with the monometallic Ni and the CuNi supported catalysts prepared with other methods, such enhanced catalytic performance was investigated to be enabled by the synergistic effect within the CuNi alloy nanoparticles. Interestingly, our bimetallic nanocatalysts could also realize efficient production of FOL from the selective hydrogenation of furfural at its aldehyde group by simply changing the solvent to methanol. Moreover, the bimetallic nanocatalysts showed good recyclability in the liquid phase hydrogenation. Our efficient and versatile CuNi alloy nanocatalysts not only provide promising candidates for effective upgrading of furfural but also broaden the application of non-noble bimetallic nanocatalysts for hydrogenative transformations.

© 2016 Elsevier B.V. All rights reserved.

## 1. Introduction

Selective conversion of renewable biomass resources into fuels and specific chemicals has attracted great attention because of the increasing demand for the development of sustainable carbon alternative to the diminishing fossil fuels [1–3]. Oxygen-containing chemicals are more attractive targets than fuels due to the higher added value and the lower consumption of hydrogen in their production. Furfural has been identified as one of the most important biomass-derived platform molecules and can be obtained from the hemicelluloses *via* acid-catalyzed hydrolysis and dehydration on a large scale [4]. Depending on the catalytic system, furfuryl alcohol (FOL) and tetrahydrofurfuryl alcohol (THFA) can be obtained

through the selective hydrogenation at the aldehyde group and further furan ring of furfural, respectively [5,6]. Besides, other chemicals such as 2-methylfuran, cyclopentanone and furan could be produced under the presence of hydrogen gas with different catalysts [7–10]. Among these transformations, the selective hydrogenation of furfural into FOL or THFA is of great importance because of their significant applications in the production of pentanediols, environmental benign solvents, industrial resins and fuel additives [11–13].

Although the toxic Cu-Cr catalyst has been successfully employed in the large-scale selective hydrogenation of furfural to FOL [14], a variety of Cr-free Cu-based [15,16] and noble metal catalysts, especially Pt [5], Ru [17,18] and Pd [19] with different particle dispersion and supports have been extensively studied. Unfortunately, many noble metal catalysts usually present dissatisfaction selectivity to FOL typically resulted by the further hydrogenolysis to 2-methyl furan and decarbonylation to furan. It was reported that

\* Corresponding author.

E-mail address: [fuweili@licp.ac.cn](mailto:fuweili@licp.ac.cn) (F. Li).

the addition of secondary metallic dopants to the metal catalysts could increase their catalytic performances [20–22], in particular, the intermetallic PtSn@SiO<sub>2</sub> nanoparticle catalyst could significantly improve the activity and selectivity in the hydrogenation of furfural to FOL in comparison to monometallic Pt@SiO<sub>2</sub> by changing furfural adsorption configuration on the intermetallic catalyst surfaces [23]. The direct conversion of furfural to THFA or hydrogenation of FOL to THFA were achieved with high selectivity and stability mainly by single noble metal and their bimetallic catalysts [6,24–29], especially Pd. Notably, the catalytic performances for the total hydrogenation of furfural to THFA were obviously enhanced over the SiO<sub>2</sub> supported M-Pd (M = Ni or Ir) alloy catalysts as compared to their monometallic counterparts, possibly ascribing to the synergy between Pd and the second metal within the small sized alloy particles through the synergistic adsorption/interaction with the furan ring and carbonyl site, respectively [27,30]. Although these precious metal-based catalysts have shown outstanding catalytic activity for the hydrogenation of furfural to THFA, the high costs and limited availability for noble metals may hinder their wide application. Many efforts have been devoted to develop efficient non-precious metal catalysts [31,32], such as Ni [27], which is highly active for the total hydrogenation of furfural to THFA. However, the leaching of monometallic Ni catalyst results in its poor reusability during the liquid phase hydrogenation reactions. Thus, it will be more economical and attractive to develop efficient, stable and environmentally benign non-noble bimetallic nanocatalysts for the hydrogenative conversion of furfural to THFA, moreover, it would be particularly attractive, if the catalyst could selectively give FOL or THFA under different reaction conditions.

Non-noble bimetallic CuNi nanocatalysts have been widely employed in many important reactions, such as CO hydrogenation [33], ethanol steam reforming [34], methane partial oxidation [35] as well as the selective hydrogenation of  $\alpha$ ,  $\beta$ -unsaturated aldehydes [36,37], which have shown enhanced catalytic activity and selectivity compared to monometallic counterparts due to their tunable composition, controllable particle dispersion and synergistic effect between different metals [38–40]. Moreover, the excellent catalytic performances of CuNi alloys are usually dependent on their high particle dispersion and homogeneous composition which are usually determined by the preparation method. Many different preparation methods including coprecipitation [41], microemulsion [42] and primarily incipient wetness impregnation methods have been used to fabricate CuNi alloy catalysts [33–37,43]. However, it is still challenging to obtain highly dispersed CuNi alloy nanoparticles with homogeneous composition (especially in the case of high metal loadings) through the impregnation protocol, due to the higher standard reduction potential for Cu (0.337 eV) than for Ni (−0.25 eV) and the poor interaction between separated metal cations [41,44]. Notably, two-dimensional layered double hydroxides (LDHs) can be controllably converted into highly dispersed supported monometallic and bimetallic nanocatalysts with homogeneous composition by topological transformation upon calcinations at reductive conditions, even in the case of high metal loadings, based on their easy-tuning compositions and atomic-level uniform dispersion of the constituents in the brucite-like layers [45–47].

As our continuing interest on the preparation of efficient and stable supported catalysts from structurally confirmed precursors [48–50], herein, a series of highly dispersed and versatile Cu<sub>x</sub>Ni<sub>y</sub> alloy supported nanocatalysts have been fabricated via the direct reduction of as-synthesized LDHs precursors and used for the selective hydrogenation of furfural into FOL and THFA. The atomically uniform distribution of metal ions in the hydrotalcite precursors promotes the synergistic interaction between Cu and Ni in the resultant CuNi alloy nanoparticle catalysts which is very crucial to enhance the catalytic performance. The optimized CuNi/MgAlO and

Cu<sub>1</sub>Ni<sub>3</sub>/MgAlO nanocatalysts showed high activity and selectivity for the hydrogenation of furfural to THFA in ethanol compared with the monometallic Ni and the CuNi supported catalysts prepared with other methods. Moreover, our versatile bimetallic nanocatalysts could realize highly efficient production of FOL only by changing the solvent to methanol. In detail, the influence of chemical composition, preparation method and particularly the reduction temperature of hydrotalcite precursor on the catalytic performance of CuNi alloy catalysts were investigated systematically. Additionally, the reaction pathways of furfural hydrogenation to THFA and the reusability of catalysts were studied.

## 2. Experimental

### 2.1. Catalyst preparation

Various Cu<sub>x</sub>Ni<sub>y</sub>MgAl-LDH hydrotalcite precursors with different Cu/Ni mole ratios (M<sup>2+</sup>/M<sup>3+</sup> = 3, x/y = 7:1, 3:1, 1:1, 1:3, 1:7, Mg/Al = 1:1) were fabricated by a modified co-precipitation method (CP) [51]. Briefly, an aqueous solution of corresponding metal nitrates (0.4 M) and the sodium hydroxide solution (1.5 M) were dropped simultaneously into sodium carbonate solution (0.1 M) and the pH of the suspension was kept at 9–10. After the suspension was aging for 20 h at 80 °C, the slurry was filtered and washed with large amount of deionized water to remove Na<sup>+</sup> ions. The resulting precipitate was dried at 80 °C for 24 h. Before catalytic performance test, the as-prepared hydrotalcite precursor was directly reduced at 600 °C for 3 h under 5% H<sub>2</sub>/Ar flow, and the obtained bimetallic nanocatalyst was denoted as Cu<sub>x</sub>Ni<sub>y</sub>/MgAlO (x/y = 7:1, 3:1, 1:1, 1:3, 1:7). Additionally, in order to investigate the effect of reduction temperature on catalytic performance, the bimetallic CuNi catalyst with Cu/Ni mole ratio of 1:1 were reduced at different temperature and marked as CuNi/MgAlO-T (T = 400 °C, 500 °C, 600 °C, 650 °C, 700 °C, 750 °C). Monometallic CuMgAl-LDH and NiMgAl-LDH were also prepared using the similar procedures and reduced respectively at 400 °C and 700 °C according to the temperature-programmed reduction (TPR) results, which were denoted as Cu/MgAlO and Ni/MgAlO. Besides, NiMgAl-LDH was also reduced at 600 °C and 800 °C to sufficiently demonstrate the advantage of bimetallic CuNi nanocatalysts. The referenced CuCo/MgAlO and NiCo/MgAlO were also prepared as the above methods and reduced at 600 °C. Other bimetallic CuNi nanoparticles (Cu: 25 wt%, Ni: 25 wt%) dispersed on different metal oxide supports, such as MgO,  $\gamma$ -Al<sub>2</sub>O<sub>3</sub>, MgAlO<sub>x</sub>, SiO<sub>2</sub>, were prepared by incipient wetness impregnation (IMP) and directly reduced at 600 °C, which were marked as CuNi/MgO-IMP, CuNi/ $\gamma$ -Al<sub>2</sub>O<sub>3</sub>-IMP, CuNi/MgAlO<sub>x</sub>-IMP and CuNi/SiO<sub>2</sub>-IMP. In this work, unless otherwise stated, Cu<sub>x</sub>Ni<sub>y</sub>/MgAlO refers to the catalysts with different Cu/Ni mole ratios reduced at 600 °C, Ni/MgAlO refers to the catalyst reduced at 700 °C.

### 2.2. Catalyst characterization

The metal contents of fresh and spent bimetallic nanocatalysts were detected by ICP-AES with a Perkin-Elmer OPTIMA 3300 DV spectrometer (Norwalk, CT, U.S.A.). Powder X-ray diffraction (XRD) measurements were performed using an X'Pert Promultipurpose diffractometer (PANalytical, Inc.) with Ni-filtered Cu K $\alpha$  radiation (0.15046 nm) at room temperature from 5° to 80° (wide angle). The nitrogen adsorption and desorption isotherms (BET) at −196 °C were recorded on a Micromeritics ASAP 2020 equipment. Prior to the tests, samples were degassed at 200 °C for 4 h. Transmission electron microscopy (TEM) and high resolution transmission electron microscope (HRTEM) were conducted in a JEM-2010 TEM with an accelerating voltage of 200 kV. X-ray pho-

toelectron spectra (XPS) analyses of the different catalysts were performed using a Thermo Fisher Scientific K-Alpha spectrometer. H<sub>2</sub> Temperature-programmed reduction (H<sub>2</sub>-TPR) was carried out on a unit DAX-7000 instrument (Huasi Technology Co., Ltd, China). Prior to testing, the fresh catalyst was pretreated at 200 °C for 1 h under Ar flow, then the temperature was increased from room temperature to 900 °C (10 °C min<sup>-1</sup>) under a continuous 3% H<sub>2</sub>/Ar flow (30 mL min<sup>-1</sup>). O<sub>2</sub> Temperature-programmed oxidation (O<sub>2</sub>-TPO) was conducted with Micromeritics AutoChem II 2920. The fresh catalyst were pretreated at the designated temperature for 0.5 h under the 5% H<sub>2</sub>/Ar flow, following by purging with high purity He, then O<sub>2</sub>-TPO profiles were recorded with the temperature increased from room temperature to 800 °C (10 °C min<sup>-1</sup>) under 2% O<sub>2</sub>/He flow (30 mL min<sup>-1</sup>). The basicity of fresh catalyst was measured by CO<sub>2</sub> temperature-programmed desorption (CO<sub>2</sub>-TPD) with Micromeritics AutoChem II 2920. The fresh catalysts were exposed to a CO<sub>2</sub> flow (30 mL min<sup>-1</sup>) at 40 °C for 1 h, and then heated linearly from 40 °C to 800 °C (10 °C min<sup>-1</sup>) in a He flow.

### 2.3. Catalytic reaction

The furfural hydrogenation reactions were carried out with various catalysts in a 100 mL stainless steel autoclave at a stirring speed of 800 rpm. In a typical catalytic test, 5 mmol of furfural, 50 mg of catalyst, 20 mL of solvent were introduced into the autoclave. After purging the reactor with pure H<sub>2</sub> for 3 times, the reactor was pressurized with pure H<sub>2</sub> to 4 MPa and heated to 150 °C. After 3 h of reaction, the autoclave was cooled to room temperature and the reaction solution was centrifuged. The reactant and liquid product samples were analyzed by gas chromatograph (Agilent GC-7890A) equipped with a capillary column AT-SE-54 (25 m × 1.5 mm × 0.1 μm) and FID detector using γ-valerolactone as an internal standard. Qualitative identification of products was achieved by GC-MS (Agilent 5975C/7890A).

## 3. Results and discussion

### 3.1. Characterization of catalysts

The XRD patterns of as-prepared Cu<sub>x</sub>Ni<sub>y</sub>MgAl-LDH precursors with different Cu/Ni mole ratios are shown in Fig. 1A. As we can see, all the XRD patterns presented characteristic peaks at 11.4°, 22.9°, 34.8°, 38.9°, 46.2°, 60.9°, 62.0°, which could be indexed to (003), (006), (012), (015), (018), (110) and (113) lattice planes of hydrotalcite, respectively [39]. After direct reduction of these hydrotalcite precursors, various supported bimetallic Cu<sub>x</sub>Ni<sub>y</sub>/MgAlO as well

as monometallic Cu/MgAlO and Ni/MgAlO nanocatalysts were obtained, as shown in Fig. 1B, all of them showed two obvious reflections at 2θ = 43.33–44.46° and 2θ = 50.44–51.85° (in the range of 2θ = 40°–55°), which were assigned to (111) and (200) crystal planes of face-centred cubic (fcc) structure [41]. As for monometallic Cu/MgAlO and Ni/MgAlO nanocatalysts, the reflection peaks at 2θ of 43.32° and 44.49° indexed to Cu(111) and Ni(111) were observed, respectively (JCPDS: 89-2838, JCPDS: 87-0712). However, the bimetallic Cu<sub>x</sub>Ni<sub>y</sub>/MgAlO catalysts presented diffraction peaks of (111) plane located at the intermediary of monometallic Cu and Ni catalysts, suggesting Cu<sub>x</sub>Ni<sub>y</sub> alloys with different compositions were successfully fabricated [44]. On the other hand, after the reduction process, the characteristic peaks of hydrotalcite precursors disappeared and some diffraction peaks corresponding to the mixed oxides with periclase structure (JCPDS: 43-1022) were observed in Fig. S1A [40,52]. Besides, these diffraction peaks were very broad, indicating the formation of hydrotalcite-derived mixed oxides with small crystallite [52]. Moreover, no peaks assigned to monometallic Cu and Ni were observed. The above XRD analysis demonstrates the direct reduction of as-synthesized hydrotalcite precursor is a facile and effective method to obtain highly dispersed and homogeneous Cu<sub>x</sub>Ni<sub>y</sub> alloys with different chemical compositions. Additionally, the concentration of Cu and Ni in the hydrotalcite derived Cu<sub>x</sub>Ni<sub>y</sub>/MgAlO nanocatalysts with different Cu/Ni mole ratios were characterized by ICP-AES and XPS as shown in Table S1. It can be seen that the real and theoretical bulk Cu/Ni ratio values were quite close. The catalysts with Cu/Ni > 1 showed a lower surface Cu/Ni ratio than the bulk. In the case of the Cu<sub>1</sub>Ni<sub>7</sub>/MgAlO catalysts, its surface Cu/Ni ratio value was larger than the bulk one, which may be due to the higher reducibility of Cu than Ni as indicated by the below H<sub>2</sub>-TPR profile (Fig. 2). As for the bimetallic Cu<sub>x</sub>Ni<sub>y</sub>/MgAlO catalysts with appropriate Cu/Ni mole ratios (x/y = 1:1, 1:3), their surface Cu/Ni ratio values were found to be similar to that of bulk, indicating the obtained CuNi alloys possessed homogeneous composition in the whole nanoparticle.

Due to the bimetallic Cu<sub>x</sub>Ni<sub>y</sub> nanocatalysts were prepared via the direct reduction of LDHs precursors, H<sub>2</sub>-TPR was used to explore the reduction behavior of as-prepared hydrotalcite precursors with different Cu/Ni mole ratios (Fig. 2). Since MgO and Al<sub>2</sub>O<sub>3</sub> could not be reduced in the studied temperature range, the present reduction peaks were attributed to the reduction process of different Cu and Ni species existed in our catalysts [53]. As for the CuMgAl-LDH precursor, a main broad hydrogen consumption peak with a maximum occurred at 425 °C, suggesting the existence of several different Cu species (Fig. 2a) [54]. The monometallic NiMgAl-LDH precursor exhibited two reduction peaks which were centered at

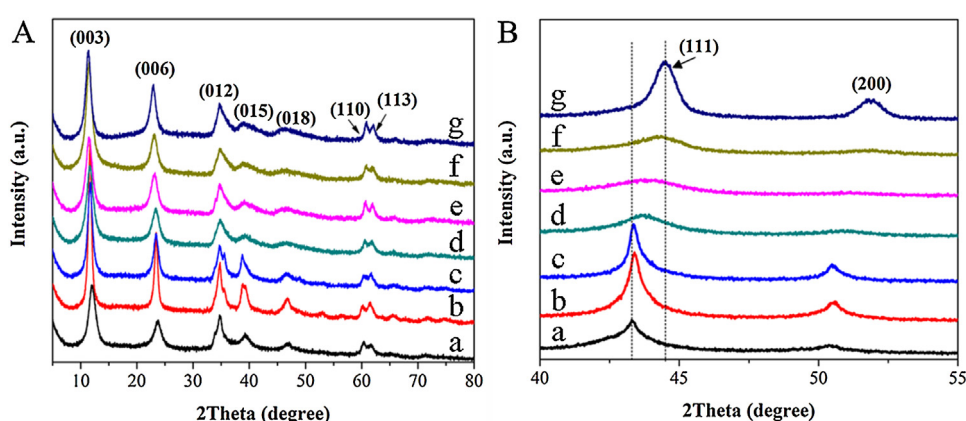


**Fig. 1.** XRD patterns of (A) as-prepared hydrotalcite precursors with different Cu/Ni mole ratios: (a) CuMgAl-LDH; (b) Cu<sub>7</sub>Ni<sub>1</sub>MgAl-LDH; (c) Cu<sub>3</sub>Ni<sub>1</sub>MgAl-LDH; (d) CuNiMgAl-LDH; (e) Cu<sub>1</sub>Ni<sub>3</sub>MgAl-LDH; (f) Cu<sub>1</sub>Ni<sub>7</sub>MgAl-LDH; (g) NiMgAl-LDH and (B) the corresponding reduced catalysts: (a) Cu/MgAlO; (b) Cu<sub>7</sub>Ni<sub>1</sub>/MgAlO; (c) Cu<sub>3</sub>Ni<sub>1</sub>/MgAlO; (d) CuNi/MgAlO; (e) Cu<sub>1</sub>Ni<sub>3</sub>/MgAlO; (f) Cu<sub>1</sub>Ni<sub>7</sub>/MgAlO; (g) Ni/MgAlO.

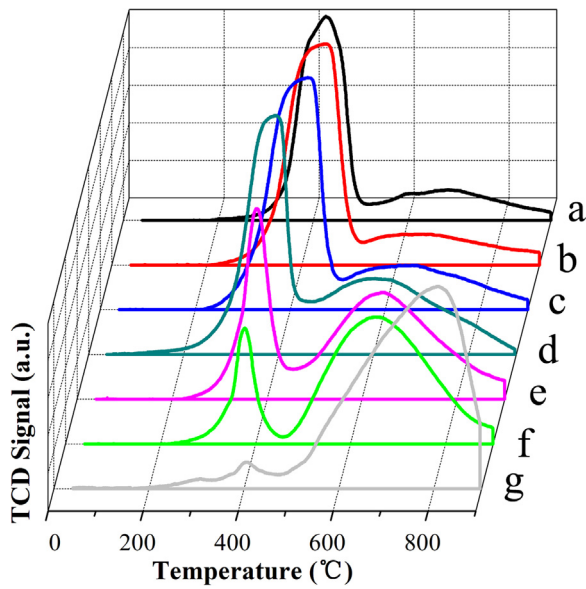


**Fig. 2.**  $\text{H}_2$ -TPR profiles of as-prepared  $\text{Cu}_x\text{Ni}_y\text{MgAl-LDH}$  hydrotalcite precursors with different Cu/Ni mole ratios: (a)  $\text{CuMgAl-LDH}$ ; (b)  $\text{Cu}_7\text{Ni}_1\text{MgAl-LDH}$ ; (c)  $\text{Cu}_3\text{Ni}_1\text{MgAl-LDH}$ ; (d)  $\text{CuNiMgAl-LDH}$ ; (e)  $\text{Cu}_1\text{Ni}_3\text{MgAl-LDH}$ ; (f)  $\text{Cu}_1\text{Ni}_7\text{MgAl-LDH}$ ; (g)  $\text{NiMgAl-LDH}$ .

408 °C and 810 °C, respectively (Fig. 2g). The former small peak was associated with the reduction of highly dispersed  $\text{NiO}$  nanoparticles, while the latter main peak was representative of the Ni species having strong interactions with the supports [2]. In the case of  $\text{Cu}_x\text{Ni}_y\text{MgAl-LDH}$  precursors with different Cu/Ni mole ratios, all  $\text{H}_2$ -TPR profiles showed two hydrogen consumption peaks, one located at 350–450 °C and another at 550–700 °C (Fig. 2b–f). Based on the integration of the peak area of the former peak, for the  $\text{Cu}_x\text{Ni}_y\text{MgAl-LDH}$  hydrotalcite with  $\text{Cu}/\text{Ni} \leq 1$  ( $\text{Cu}/\text{Ni} = 1:1, 1:3, 1:7$ ), the amount of  $\text{H}_2$  consumption was higher than that required for the complete reduction of Cu species, indicating the former reduction peak was assigned to the reduction processes of  $\text{Cu}(\text{II})$  to  $\text{Cu}(0)$  and a small amount of  $\text{Ni}(\text{II})$  to  $\text{Ni}(0)$ , the latter broad reduction peak was characteristic of the reduction process of  $\text{Ni}(\text{II})$  to  $\text{Ni}(0)$ . While for the precursor with  $\text{Cu}/\text{Ni} > 1$  ( $\text{Cu}/\text{Ni} = 3:1, 7:1$ ), the corresponding amount of  $\text{H}_2$  consumption was slightly lower than that required for the complete reduction of Cu species, suggesting the former hydrogen consumption peak was assigned to the reduction of Cu species and the latter peak was mainly attributed to the reduction of Ni species. Additionally, it can be noted that an obvious increase in the reducibility of metal species when the combination of Cu and Ni were supported on oxides. Especially for  $\text{Ni}^{2+}$  species, the reduction peak of which migrated to lower temperature with Cu doped into the LDHs precursors. This phenomenon indicates there is strong synergistic interaction between Cu and Ni in our CuNi alloy catalysts, and the addition of Cu obviously promotes the dispersion of Ni metal, which is also confirmed by above XRD patterns (Fig. 1B) [39]. Notably,  $\text{CuNiMgAl-LDH}$  hydrotalcite precursor with Cu/Ni mole ratio of 1:1 exhibited the lowest reduction temperature for Ni species as compared with other  $\text{Cu}_x\text{Ni}_y\text{MgAl-LDH}$ , which seemed to assume that there were strongest interaction between Cu and Ni [36,54].

In order to further investigate the effect of reduction temperature on the structure of bimetallic CuNi nanocatalysts, the  $\text{CuNiMgAl-LDH}$  ( $\text{Cu}/\text{Ni} = 1:1$ ) catalyst precursor was taken as an example and activated at different temperature from 400 °C to 750 °C. The XRD diffraction patterns of resultant  $\text{CuNi/MgAlO-T}$  catalysts are summarized in Fig. 3. It can be seen that all bimetallic nanocatalysts showed three characteristic diffraction peaks at

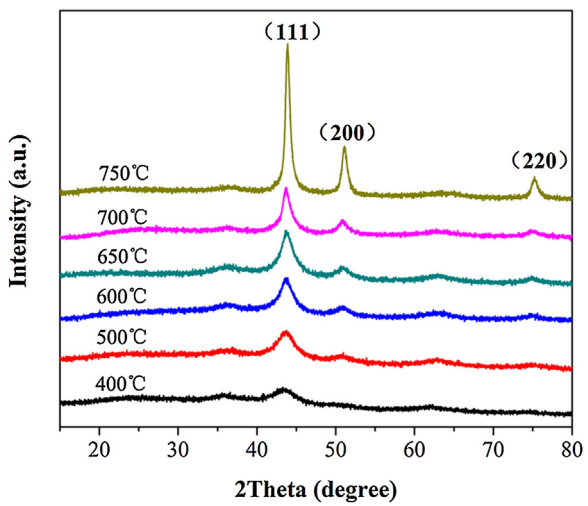


**Fig. 3.** XRD patterns of the bimetallic  $\text{CuNi/MgAlO-T}$  nanocatalysts with different reduction temperature.

$2\theta = 43.81^\circ, 51.06^\circ$  and  $75.16^\circ$  which were ascribed to the (111), (200) and (220) crystal planes of CuNi alloys, respectively [44]. Meanwhile, the diffraction peaks assigned to the hydrotalcite-derived mixed oxides with periclase structure (JCPDS: 43-1022) were also observed, which are shown in Fig. S1B. Obviously, CuNi alloy nanoparticles have been formed even at a low temperature of 400 °C, albeit its very weak diffraction peak and poor crystallinity, which was also confirmed by EDS line spectra and the  $\text{H}_2$ -TPR results (Figs. S2, 2 d). It is generally accepted that the intensity of diffraction peak of supported bimetallic nanoparticles is correlated with particle dispersion to some extent. As the reduction temperature increasing, more intense characteristic diffraction peaks of CuNi alloys were detected in the  $\text{CuNi/MgAlO-T}$  catalysts, suggesting the gradual increase of particle size and the formation of well-defined bimetallic nanoparticles, which were also consistent with the below TEM results (Fig. 4). Moreover, the physicochemical properties of the bimetallic  $\text{CuNi/MgAlO-T}$  nanocatalysts with different reduction temperature were investigated by ICP-AES and BET, which are summarized in Table S2. Notably, the metal loading of both Cu and Ni was about 25 wt%, indicating the preparation method of direct reduction of hydrotalcite precursor is beneficial to obtain CuNi alloys with high metal loadings.

Generally, the reduction temperature of precursors has significant influences on the particle dispersion of the supported nanoparticle catalysts. TEM characterization was conducted to investigate the structure and morphology of the bimetallic nanocatalysts. It can be seen in Fig. 4 that the obtained  $\text{CuNi/MgAlO-T}$  nanocatalysts with different reduction temperature from 400 °C to 750 °C still partially maintained plate-like structure of their hydrotalcite precursors. Highly dispersed nanoparticles with an average size of 4–5 nm were distributed uniformly in the matrix of the catalysts reduced at different temperature from 400 °C to 600 °C (Fig. 4A–C). However, many large particles were observed in the supports as the activation temperature increased to 700 °C, which may be ascribed to particle agglomeration or sintering caused by high temperature (Fig. 4E). These TEM results indicate the utilization of hydrotalcite precursors is reasonable to prepare highly dispersed CuNi alloys in the case of high metal loadings by selecting appropriate reduction temperature.

In the HRTEM image of  $\text{CuNi/MgAlO}$  (Fig. 5A), a typical lattice spacing of 0.206 nm was detected, which was assigned to (111) plane of the face-centred cubic (fcc) CuNi alloy. The distribution of the element Cu and Ni within one individual nanoparticle was detected by HADDF-STEM and EDS line scan spectra (Fig. 5B–C).

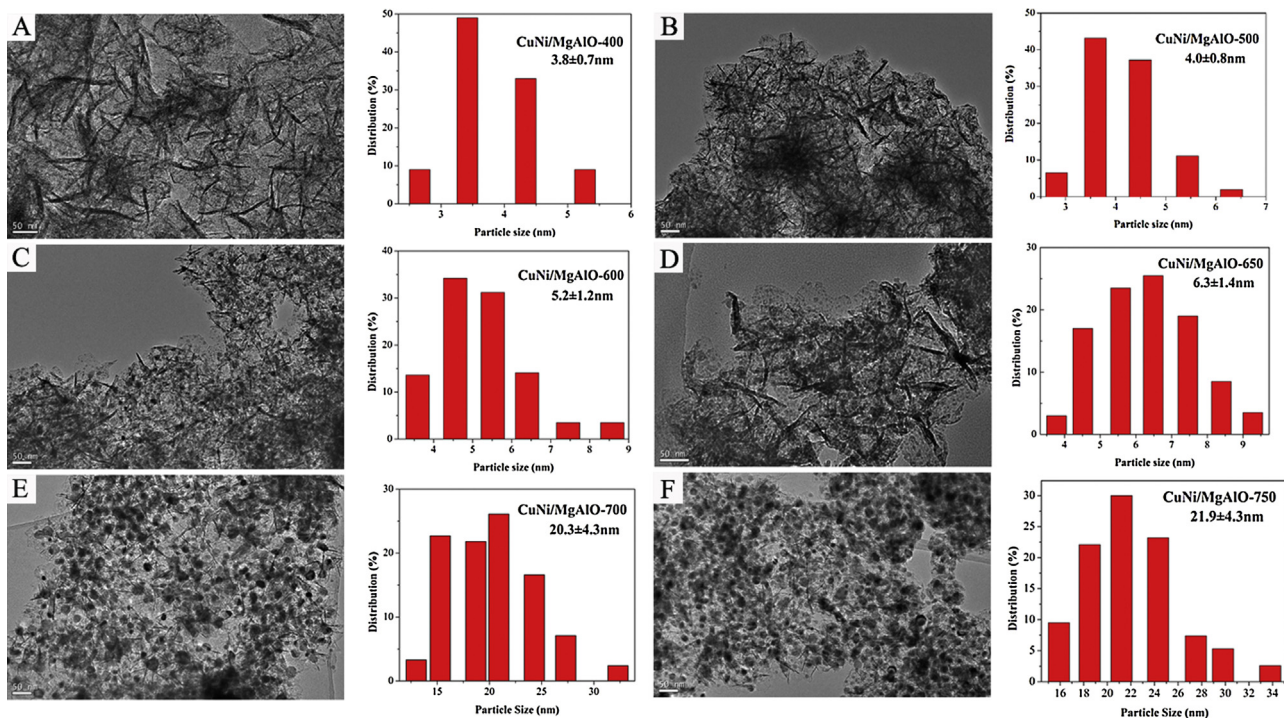


**Fig. 4.** Typical TEM images and the corresponding particle size distribution of the bimetallic CuNi/MgAlO-T nanocatalysts with different reduction temperature: (A) CuNi/MgAlO-400; (B) CuNi/MgAlO-500; (C) CuNi/MgAlO-600; (D) CuNi/MgAlO-650; (E) CuNi/MgAlO-700; (F) CuNi/MgAlO-750.

Similar distribution profiles of Cu and Ni were observed, suggesting their homogeneous distribution and the strong interaction between Cu and Ni in the well-defined CuNi alloys, which was also confirmed by XRD pattern (Fig. 3). Besides, the elemental mapping analysis based on EDS exhibited a homogeneous distribution of copper, nickel, magnesium, aluminum and oxygen elements in the bimetallic nanocatalysts, respectively, which was possibly originated from the atomically uniform dispersion of metal ions in the hydrotalcite precursors (Fig. 5D).

### 3.2. Catalytic performances

**Table 1** presents the catalytic performances of various monometallic and bimetallic nanocatalysts prepared by different methods for the hydrogenation of furfural in ethanol. Initially, a series of bimetallic Cu<sub>x</sub>Ni<sub>y</sub>/MgAlO nanocatalysts with different Cu/Ni mole ratios were used to investigate the influence of chemical composition on the selectivity of furfural hydrogenation. It was found that the bimetallic CuNi/MgAlO nanocatalyst fabricated by the direct reduction of hydrotalcite precursors showed the highest selectivity of 95% to tetrahydrofurfuryl alcohol (THFA) derived from total hydrogenation of furfural (entry 4). While the C=O partial hydrogenation product furfuryl alcohol (FOL) became dominated in the products with the Cu/Ni ratio increasing in bimetallic catalysts (entries 1–3). Notably, in the case of monometallic Cu/MgAlO catalyst, an extremely high selectivity of 99% to FOL was obtained, which revealed Cu was responsible for the selective hydrogenation of C=O in furfural [16,55]. However, as for the Ni-rich bimetallic nanocatalysts, a considerably high selectivity (93%) of THFA was also obtained over the Cu<sub>1</sub>Ni<sub>3</sub>/MgAlO catalysts (entry 5). Unfortunately, as the content of Ni further increased, Cu<sub>1</sub>Ni<sub>7</sub>/MgAlO catalyst showed an obvious decline in the selectivity to THFA (21%), which might be ascribed to the strong metal-support interaction decreased the reduction degree of active metal species and resulted in the diminishing of hydrogenation activity [56] as evidenced by TPR profile (Fig. 2f). The referenced monometallic Ni/MgAlO gave a

**Table 1**  
The hydrogenation of furfural with various catalysts in ethanol<sup>a</sup>.

Entry	Catalyst	Conversion (%)	Selectivity (%)		
			FOL	THFA	Others <sup>c</sup>
1	Cu/MgAlO	>99	>99	0	0
2	Cu <sub>7</sub> Ni <sub>1</sub> /MgAlO	>99	80	20	0
3	Cu <sub>3</sub> Ni <sub>1</sub> /MgAlO	>99	20	74	6
4	CuNi/MgAlO	>99	0	95	5
5	Cu <sub>1</sub> Ni <sub>3</sub> /MgAlO	>99	0	93	7
6	Cu <sub>1</sub> Ni <sub>7</sub> /MgAlO	>99	74	21	5
7	Ni/MgAlO	>99	25	65	10
8 <sup>b</sup>	Cu/MgAlO + Ni/MgAlO	>99	62	33	5
9	MgAl-LDO	28	61	0	39
10	NiCo/MgAlO	90	91	3	6
11	CuCo/MgAlO	>99	50	18	32
12	5% Ru/C	>99	0	81	19
13	CuNi/MgO-IMP	54	>99	0	0
14	CuNi/γ-Al <sub>2</sub> O <sub>3</sub> -IMP	90	67	0	33
15	CuNi/SiO <sub>2</sub> -IMP	>99	70	17	13
16	CuNi/MgAlO <sub>x</sub> -IMP	>99	77	12	11
17	Blank	0	0	0	0

<sup>a</sup> Reaction conditions: furfural 5 mmol, ethanol 20 mL, catalyst 0.05 g, 150 °C, 3 h, H<sub>2</sub> 4 MPa.

<sup>b</sup> Physical mixture of 0.025 g of monometallic Ni and 0.025 g Cu catalysts.

<sup>c</sup> Others refer to by-products mainly contain 1,2-pentanediol, 1,5-pentanediol, 2-furaldehyde diethyl acetal and other not detected.

low selectivity of 65% to THFA (entry 7). The XPS result suggested that the nature of metallic Ni species was sensitive to oxygen and this might be one of the factors that leading to the lower catalytic activity (Fig. S4). Other Ni/MgAlO-T catalysts with different reduction temperature (T = 600 °C, 800 °C) were also used for the total hydrogenation of furfural and they all displayed inferior catalytic performances (the selectivity of THFA were 13% and 52%, respectively, entries 2–3, Table S3). The above results indicate bimetallic Cu<sub>x</sub>Ni<sub>y</sub>/MgAlO nanocatalysts with appropriate Cu/Ni ratios can give much higher yield of THFA from the total hydrogenation of furfural than monometallic Ni. In order to further investigate the

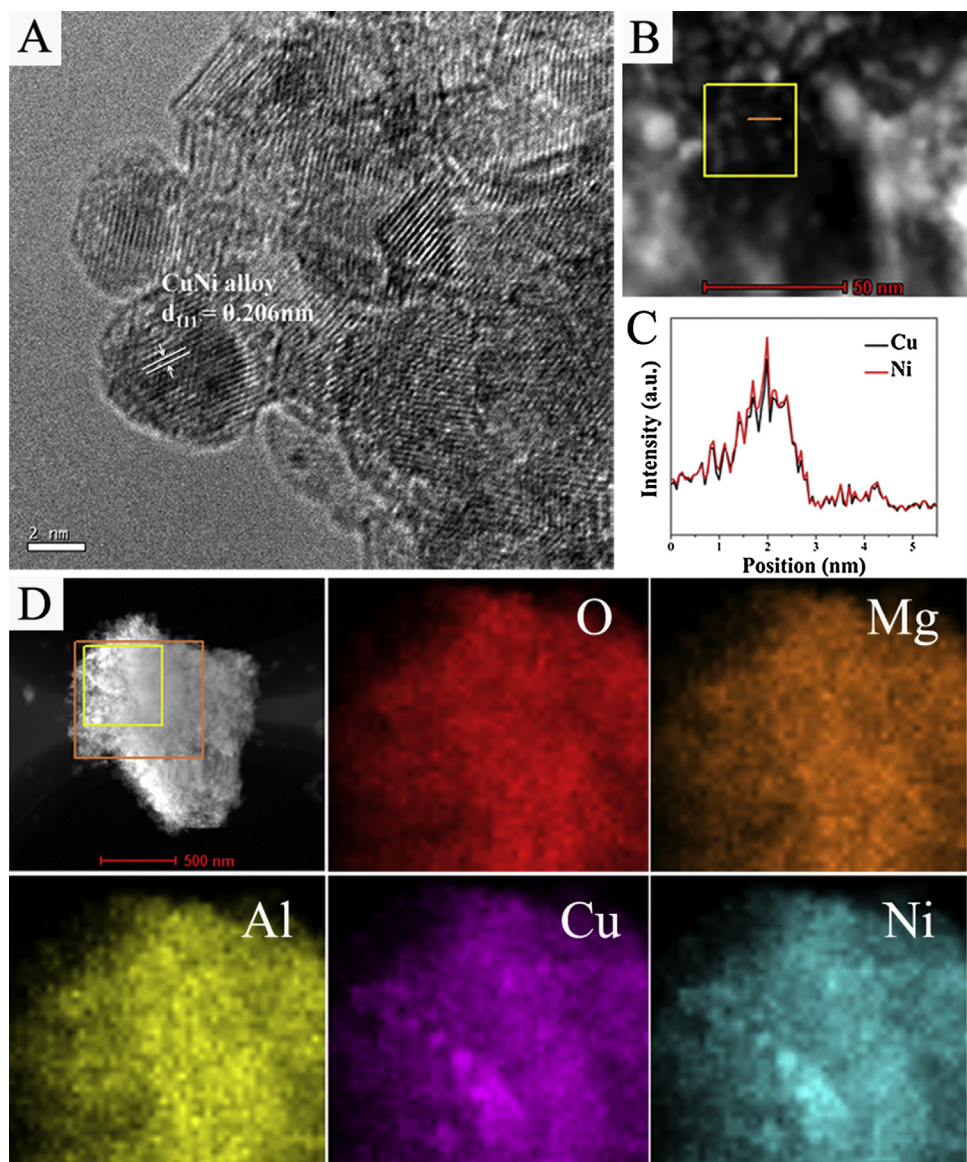


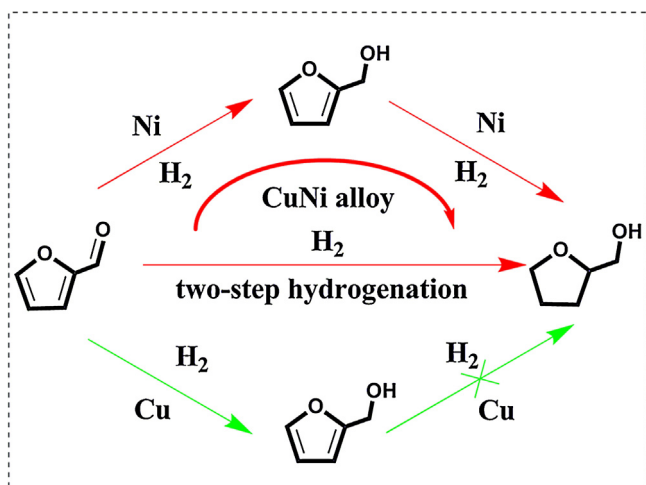
**Fig. 5.** Structure characterizations of the bimetallic CuNi/MgAlO: (A) HRTEM image; (B) HADDF-STEM image; (C) EDS line spectra along the red line in B; (D) HADDF-STEM image and elemental maps. (For interpretation of the references to color in this figure legend, the reader is referred to the web version of this article.)

superior activity of bimetallic catalysts, another control experiment was conducted where a physical mixture of Cu/MgAlO and Ni/MgAlO was used as the catalyst for such a transformation under the same reaction conditions. Only 33% selectivity of THFA was obtained (entry 8), which revealed that the synergistic interaction between Cu and Ni within the supported CuNi alloys played crucial roles in realizing outstanding catalytic performance for the furfural total hydrogenation. As expected, single support MgAl-LDO catalyst gave 28% conversion of furfural at identical reaction conditions and only some 2-furaldehyde diethyl acetal was observed from the side reaction between furfural and ethanol solvent. Interestingly, the referenced NiCo/MgAlO showed 90% conversion of furfural but 91% selectivity to FOL instead of THFA (entry 10), while CuCo/MgAlO catalyst gave 50% selectivity to FOL and 18% to THFA, and small amounts (18% of selectivity) of 1,2-pentanediol and 1,5-pentanediol were also obtained under the same reaction conditions (entry 11). Besides, the traditional hydrogenation catalyst Ru/C only gave 81% selectivity of THFA (entry 12). These results are likely to reveal that our uniform and well-dispersed  $\text{Cu}_x\text{Ni}_y$  nanocatalysts

with proper chemical compositions are outstanding candidates for the total hydrogenation of furfural to THFA in ethanol.

As is well known, the preparation method has a great effect on the particle dispersion of heterogeneous catalysts, which is closely associated with the catalytic performance. Using the traditional incipient wetness impregnation (IMP) method usually gets large and non-uniform CuNi alloy nanoparticles, especially in the case of high metal loadings. As expected, these bimetallic CuNi catalysts fabricated by IMP gave much lower selectivity of THFA (Table 1, entries 13–16), possibly ascribing to the poor dispersion of metal nanoparticles, as revealed by TEM characterization (Fig. S5).

In order to gain more insight into the catalytic system of furfural hydrogenation in ethanol, various reaction parameters such as temperature and  $\text{H}_2$  pressure were optimized using our bimetallic CuNi/MgAlO nanocatalysts which are illustrated in Table S4. With the reaction temperature increased from 100 °C to 150 °C (Table S4, entries 1–4), the selectivity of THFA increased sharply from 5% to a maximum of 95%, while the selectivity to FOL presented an opposite trend. If increasing the reaction temperature further to 170 °C (entry 5), the selectivity of THFA began to decrease (87%), and sev-



**Scheme 1.** The reaction pathways of furfural hydrogenation in ethanol over monometallic Cu/MgAlO, Ni/MgAlO and bimetallic CuNi/MgAlO nanocatalysts.

eral by-products such as 1,2-pentanediol and 1,5-pentanediol were observed. Thus, 150 °C may be the desired reaction temperature for the high selectivity to THFA. On the other hand, the selectivity of THFA increased obviously from 58% to 95% as H<sub>2</sub> pressure improved from 3 MPa to 4 MPa, however, a slight decrease in the selectivity of THFA (92%) was obtained after enhancing H<sub>2</sub> pressure up to 5 MPa (entries 6–7). Additionally, the time course of reaction was explored where an obvious increase in the selectivity to THFA was observed over CuNi/MgAlO with the reaction time from 0.5 h to 3 h, while the corresponding selectivity to FOL decreased significantly (entries 8–11). This phenomenon suggests that the transformation of furfural to THFA is a consecutive two-step hydrogenation process via the FOL intermediate over our CuNi nanocatalyst.

With the above results achieved, the reaction pathways of furfural hydrogenation to THFA in ethanol over our monometallic and bimetallic nanocatalysts are proposed in **Scheme 1**. Present bimetallic CuNi nanocatalyst exhibits a continuous two-step hydrogenation process. In the case of monometallic Ni catalyst, the two-step hydrogenation process still exists (Table S4, entries 15–18). However, the bimetallic CuNi nanocatalysts presented higher catalytic performances than monometallic Ni catalyst. As for monometallic Cu catalyst, it is only active for the selective hydrogenation of furfural at the aldehyde group to produce FOL.

It is generally considered that the activation temperature has an important effect on the microstructure of the resultant nanoparticles supported catalyst, such as particle dispersion, surface composition and acid-base properties, which are directly associated with the catalytic activity and selectivity [57]. Based on the above experiment results, the CuNi/MgAlO-T (T = 400 °C, 500 °C, 600 °C, 650 °C, 700 °C, 750 °C) catalysts were representatively used to elucidate such influence, as shown in **Fig. 6**, the selectivity to THFA increased gradually from 81% over the CuNi/MgAlO-400 to a maximum of 95% over the CuNi/MgAlO-600 and then sharply dropped to 2% with the catalysis of CuNi/MgAlO-750. Such a remarkable change of selectivity inspired us to further investigate the structure–activity relationships in our bimetallic CuNi catalytic system.

The above CuNi/MgAlO-T nanocatalysts reduced at different reduction temperature were used to explore their intrinsic catalytic performances at a low conversion of furfural. Given that the characteristic of a two-step hydrogenation process involved in our bimetallic catalytic system, much milder reaction conditions are necessary to evaluate the TOF values of the two steps, respectively, which are illustrated in **Table 2**. It can be seen that the

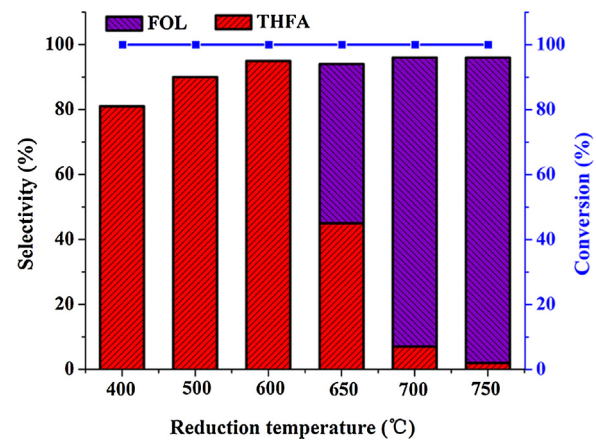


**Fig. 6.** Effect of reduction temperature on the hydrogenation of furfural over bimetallic CuNi/MgAlO-T nanocatalysts. Reaction conditions: furfural 5 mmol, ethanol 20 mL, catalyst 0.05 g, 150 °C, 3 h, H<sub>2</sub> 4 MPa.

**Table 2**

TOF values of the two-step hydrogenation of furfural over bimetallic CuNi/MgAlO-T and monometallic Cu and Ni nanocatalysts in ethanol.

Entry	Catalyst	TOF <sub>C=O</sub> (h <sup>-1</sup> ) <sup>a</sup>	TOF <sub>C=C</sub> (h <sup>-1</sup> ) <sup>b</sup>
1	CuNi/MgAlO-400	142.26	22.28
2	CuNi/MgAlO-500	124.09	24.44
3	CuNi/MgAlO-600	115.24	34.45
4	CuNi/MgAlO-650	69.46	16.27
5	CuNi/MgAlO-700	53.54	13.9
6	CuNi/MgAlO-750	19.9	0
7	Cu/MgAlO	71.29	0
8	Ni/MgAlO	33.9	23.83

Reaction conditions: <sup>a</sup> furfural 5 mmol, ethanol 20 mL, catalyst 0.005 g, 140 °C, 0.5 h, H<sub>2</sub> 4 MPa. <sup>b</sup> furfuryl alcohol 5 mmol, 1 h. TOF is defined as the mol of FOL or THFA generated per metal site per hour, metal sites refer to the total amount of Cu and Ni sites determined by ICP-AES.

TOF<sub>C=O</sub> values belonging to the hydrogenation at aldehyde group of furfural to FOL are obviously larger than that of FOL hydrogenation to THFA (TOF<sub>C=C</sub>) in all nanocatalysts, which indicates the latter reaction process may be the rate-determining step for the total hydrogenation of furfural over our bimetallic CuNi nanocatalysts. Notably, both TOF<sub>C=O</sub> and TOF<sub>C=C</sub> assigned to the bimetallic catalysts are obviously larger than that of monometallic counterparts, which suggested the synergistic effect between Cu and Ni improved the catalytic performance. Considering the decisive role of the process of FOL to THFA, we attempted to correlate the TOF<sub>C=C</sub> values and THFA selectivity with particle sizes of bimetallic CuNi nanocatalysts, which is shown in **Fig. 7** (the corresponding average nanoparticle size was illustrated in **Fig. 5**). Clearly, the correlation of both TOF<sub>C=C</sub> values and selectivity to THFA with CuNi alloy sizes exhibited volcano-shaped variations where the largest TOF<sub>C=C</sub> values of 34.45 h<sup>-1</sup> and THFA selectivity of 95% were observed over the catalyst possessing an average size of 5.2 nm and reduced at 600 °C. Based on these investigations, it seems that the reaction process of furfural hydrogenation to THFA is structure-sensitive in which particle size of CuNi alloy nanocatalyst is of great importance to control the selectivity of THFA.

On the other hand, the surface chemical composition of heterogeneous catalysts is a key factor to influence catalytic activity and selectivity. As evident from the XPS analyses of CuNi/MgAlO-T (Table S5), it was found that their surface Cu/Ni mole ratio elevated from 0.615 to 1.538 with the increase of reduction temperature from 400 °C to 750 °C, while the bulk Cu/Ni ratio was about 1.0 in all catalysts. Especially for the catalysts reduced at high temperature (650 °C, 700 °C, 750 °C), their surface ratios of Cu/Ni were larger than that of bulk ones (Table S5, entries 4–6). This phenomenon

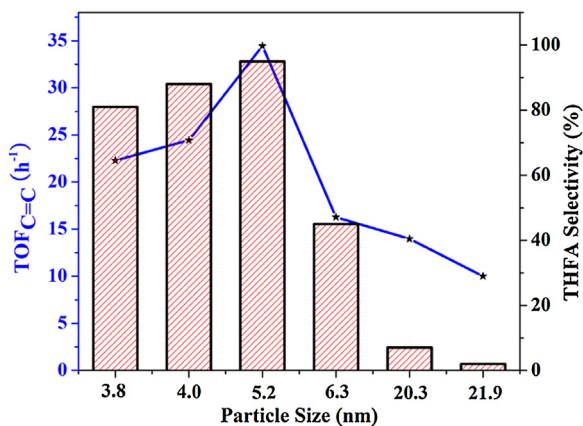


**Fig. 7.** TOF<sub>C=C</sub> values and selectivity of THFA as a function of particle size of bimetallic CuNi/MgAlO-T catalyst. Reaction conditions: TOF<sub>C=C</sub> (h<sup>-1</sup>) values are calculated at the conditions of Table 2 and the THFA selectivity is calculated with the same conditions of Fig. 6.

suggested that Cu segregated into the nanoparticle surface gradually to form Cu-rich CuNi alloys as the reduction temperature increased, which might also explain the gradually enhanced selectivity to FOL in the case of bimetallic CuNi catalysts reduced by higher temperature (Table S5, entries 1–6), because the Cu catalytic sites were believed to be selectively active toward the hydrogenation of aldehyde moiety and inert for the furan ring activation [16,55]. However, as for the catalyst reduced at 600 °C, its surface Cu/Ni ratio is 0.947, suggesting the CuNi alloy has relatively homogeneous composition. That is believed to be an important factor that determines such outstanding catalytic performance of the optimized CuNi/MgAlO-600 catalyst for the total hydrogenation of furfural to THFA.

Besides, the correlation between the selectivity of THFA and the base concentration of CuNi/MgAlO-T catalysts with different reduction temperature was taken according to the CO<sub>2</sub>-TPD results and summarized in Fig. S3. It was found that the highest selectivity of THFA occurred at the total base concentration of 0.7 mmol g<sup>-1</sup> (corresponding to the CuNi/MgAlO-600), indicating an appropriate amount of surface basicity could facilitate the high selectivity of THFA (Fig. S3B). Moreover, the excessive basic concentration may lead to side reactions. For example, 6.8–9.6% yield of 1,2-pentanediol and 1,5-pentanediol derived from the furan ring opening secondary reaction were observed over both CuNi/MgAlO-400 and CuNi/MgAlO-500, which might be caused by the high concentration of basic sites in these two catalysts (Fig. S3A) [58]. In addition, other several side reactions such as hydrogenolysis and acetalization which are catalyzed by acidic sites could be suppressed due to the presence of proper basic sites in the CuNi catalysts [5]. As was mentioned above, the CuNi nanoparticles supported on acidic oxides presented lower selectivity to THFA (Table 1, entries 14–15).

The metal surface area and particle dispersion of monometallic Cu and Ni and bimetallic CuNi/MgAlO-T nanocatalysts are listed in Table S2. It was found that the metal surface area and particle dispersion of bimetallic CuNi/MgAlO-T decreased gradually with the reduction temperature increasing from 400 °C to 750 °C. Especially for the bimetallic catalyst reduced at a high temperature (such as 700 °C and 750 °C), a low metal surface area and particle dispersion were observed, which might lead to the decrease of selectivity of THFA during furfural hydrogenation, this result is in agreement with Fig. 7. Notably, both the metal surface area and particle dispersion of CuNi/MgAlO-600 were higher than that of monometallic Ni/MgAlO, this might be an important factor that resulting in the high catalytic performance of CuNi alloy nanocatalyst. Besides, the

reduction degrees of copper and nickel species in the bimetallic CuNi/MgAlO-T and monometallic Cu and Ni nanocatalysts were calculated based on the amount of O<sub>2</sub> consumption in O<sub>2</sub>-TPO (Fig. S8) and the particle composition determined by XRD patterns (assuming that Cu<sup>0</sup> + 1/2O<sub>2</sub> → CuO, Ni<sup>0</sup> + 1/2O<sub>2</sub> → NiO) [40]. As shown in Table S2, it can be seen that the reduction degree of Cu and Ni species increased gradually with the increase of reduction temperature. Moreover, the bimetallic CuNi/MgAlO-600 showed higher reduction degrees than the monometallic catalysts in both case of Cu and Ni species. Therefore, it is believed that the high catalytic activity and selectivity of our bimetallic CuNi nanocatalysts for the total hydrogenation of furfural to THFA is not only attributed to the synergistic effect between Cu and Ni, but also closely related to the highly dispersed microstructure with homogeneous composition and suitable surface basicity.

Solvent effects are very important in heterogeneous catalysis which can greatly affect the activity and selectivity in many specific reactions. Herein, various solvents were investigated using CuNi/MgAlO as the catalyst and the catalytic results are summarized in Table S6. Interestingly, an obvious change in the selectivity to THFA or FOL with different solvents was found in the hydrogenation of furfural, especially in the case of methanol where a high selectivity of 95% to FOL instead of THFA was achieved under the same reaction conditions (Table S6, entry 1). This result implies that solvent has a significant effect on the selectivity for furfural hydrogenation in our catalyst system. In order to further explore the role of methanol in the hydrogenation of furfural to FOL, a series of mixed solvents with different volume ratio of methanol and ethanol were used for furfural hydrogenation, the corresponding catalytic results are displayed in Table S7. The selectivity of FOL increased linearly with the increase of methanol volume in the mixed solvents, implying that the stronger adsorption of methanol on the present catalytic sites suppressed their activity for ring hydrogenation of furfural to some extent. Similar solvent effects were also observed in other reactions [59–61], and Al-Mawlawi et al. investigated the dissociation adsorption of alcohol molecules on different metal films of Ni, Pd, Al and found the Ni film taken up 1.9 times more methanol than ethanol in the adsorption process [59]. Accordingly, it seems reasonable to suggest a stronger adsorption of methanol than ethanol on the surface of Ni sites which is specifically active for furan ring hydrogenation in our bimetallic Cu<sub>x</sub>Ni<sub>y</sub> catalysts. Thus, a competitive adsorption between solvent and furan ring for the available effective metal sites occurred and resulted in the decrease of hydrogenation ability of furan ring. More interestingly, similar solvent effects also existed in other Cu<sub>x</sub>Ni<sub>y</sub> catalysts with different chemical compositions (Table S6, entries 10–11), the Cu<sub>1</sub>Ni<sub>3</sub>/MgAlO catalyst showed high selectivity of 94% to FOL in methanol. Thus, it will be very attractive that such a high selectivity of FOL or THFA can be obtained over the versatile bimetallic CuNi nanocatalyst via the simple switch of different alcoholic solution. Subsequently, the reaction conditions were further optimized for the hydrogenation of furfural in methanol. It can be seen in Table 3 that an extremely high selectivity of 99% to FOL could be obtained in mild reaction conditions over the representative CuNi/MgAlO catalyst (entry 5). Besides, the bimetallic CuNi catalyst showed obviously higher activity compared to the monometallic Cu and Ni (entries 1–3), which further demonstrated the important role of synergistic effect between Cu and Ni in these two reaction systems. Interestingly, the utilization of solvent effects seems to be an effective and simple method to control the selectivity of target products in upgrading biomass-derived compounds, it would be also attractive to explore the detailed mechanisms behind the solvent effects.

After centrifugation and washing with solvent, the spent bimetallic Cu<sub>x</sub>Ni<sub>y</sub> nanocatalysts could be readily used in the next catalytic cycles. As shown in Fig. 8A, in the case of furfural total

**Table 3**

The hydrogenation of furfural over bimetallic CuNi/MgAlO and monometallic Cu and Ni nanocatalysts in methanol<sup>a</sup>.

Entry	Catalyst	Conversion (%)	Selectivity (%)		
			FOL	THFA	Others <sup>d</sup>
1	Cu/MgAlO	26	91	0	9
2	CuNi/MgAlO	58	>99	0	0
3	Ni/MgAlO	12	80	0	20
4 <sup>b</sup>	CuNi/MgAlO	79	>99	0	0
5 <sup>c</sup>	CuNi/MgAlO	>99	>99	0	0

<sup>a</sup> Reaction conditions: furfural 5 mmol, methanol 20 mL, catalyst 0.01 g, 100 °C, 1 h, H<sub>2</sub> 4 MPa.

<sup>b</sup> 3 h.

<sup>c</sup> 4 h.

<sup>d</sup> Others include substances not detected.

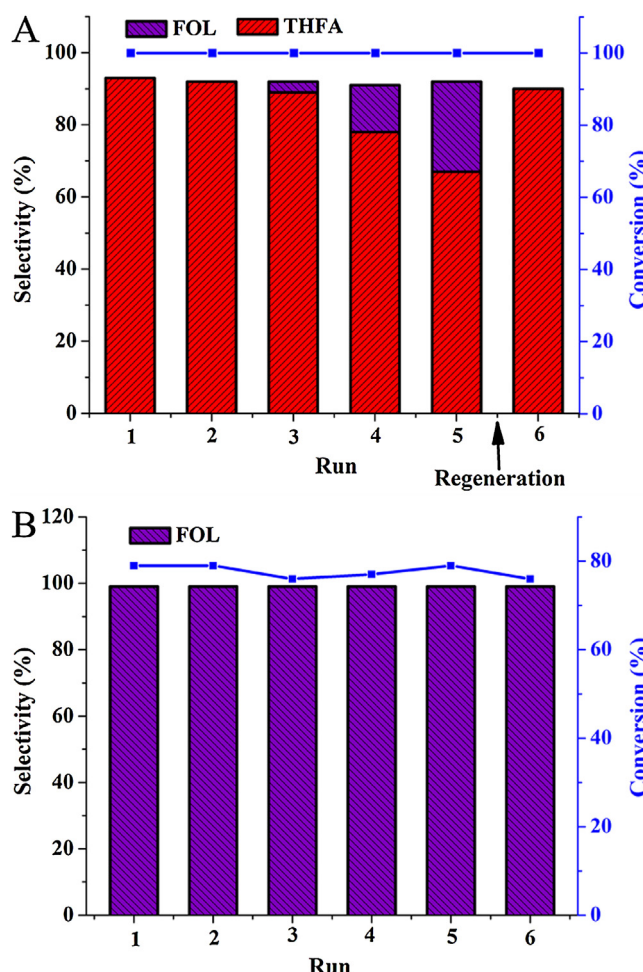


**Fig. 8.** Reusability of Cu<sub>1</sub>Ni<sub>3</sub>/MgAlO and CuNi/MgAlO catalysts for the hydrogenation of furfural in ethanol and methanol, respectively. Reaction conditions: (A) furfural 5 mmol, ethanol 20 mL, catalyst (Cu<sub>1</sub>Ni<sub>3</sub>/MgAlO) 0.05 g, 150 °C, 3 h, H<sub>2</sub> 4 MPa, (B) furfural 5 mmol, methanol 20 mL, catalyst (CuNi/MgAlO) 0.01 g, 100 °C, 3 h, H<sub>2</sub> 4 MPa.

hydrogenation in ethanol, the representative Cu<sub>1</sub>Ni<sub>3</sub>/MgAlO catalyst showed a full conversion of furfural in the consecutive five catalytic runs with a gradual decrease of the hydrogenation ability. The chemical composition of the spent Cu<sub>1</sub>Ni<sub>3</sub>/MgAlO catalyst was checked by ICP-AES (Table S8), it was found that slight leaching of Cu and Ni metals occurred in the spent catalyst. In order to demonstrate the heterogeneous nature of the reaction of furfural hydrogenation, a hot filtration test was performed using the Cu<sub>1</sub>Ni<sub>3</sub>/MgAlO catalyst where the hot reaction mixture was filtered

after the reaction for 1 h at 150 °C, 4 MPa H<sub>2</sub>. Then the reaction was continued without a catalyst after adding the fresh reactants into the filtrate under the identical conditions and no additional conversion of furfural and FOL was observed, indicating the leached metals could be excluded as the catalytically active species. Besides, the TEM images of the spent Cu<sub>1</sub>Ni<sub>3</sub>/MgAlO catalyst showed no obvious aggregation of particles compared with the fresh catalyst (Fig. S6). And the XRD pattern of the spent catalyst was similar to the fresh sample (Fig. S7A). To our delight, it could be regenerated after the fifth cycle by activating in 5%H<sub>2</sub>/Ar for 1 h at 600 °C, and a high selectivity of 90% of THFA could be obtained. Moreover, as for the hydrogenation of furfural in methanol (Fig. 8B), another optimal CuNi/MgAlO nanocatalyst could be recycled up to six times without obvious loss of the reactivity and selectivity, which indicates the high stability of our bimetallic CuNi nanocatalyst, as suggested by the detailed characterization of TEM, XRD and XPS (Figs. S6, S7 and S9).

#### 4. Conclusions

In summary, we have developed a series of highly dispersed and stable CuNi alloy nanoparticle supported catalysts via the simple direct reduction of as-synthesized Cu<sub>x</sub>Ni<sub>y</sub>MgAl-LDH hydroxide precursors. The optimized CuNi/MgAlO and Cu<sub>1</sub>Ni<sub>3</sub>/MgAlO nanocatalysts, which were reductively treated at 600 °C, showed excellent catalytic performance for the hydrogenation of furfural to THFA in ethanol in comparison with the monometallic Ni. Such promoting effect in terms of catalytic activity and THFA selectivity was investigated to be significantly enabled by the synergistic effect within the supported CuNi alloy nanoparticles. Systematic investigations revealed that the chemical composition, preparation method and reduction temperature of the catalytic precursors greatly affected their properties. Particularly, an appropriate reduction temperature of hydroxide precursor was closely related to the high particle dispersion and homogeneous composition of the CuNi alloys as well as the proper surface basicity of the resultant catalyst, which play crucial roles in achieving excellent catalytic performances. Interestingly, the selectivity for furfural hydrogenation could be perfectly switched from THFA to FOL only by changing the solvent to methanol. Moreover, the bimetallic nanocatalysts showed good stability during the consecutive catalytic runs. These efficient and versatile CuNi alloy nanocatalysts are not only promising candidates for effective upgrading of biomass-derived furfural, but also provide useful guidance for rational design of non-noble bimetallic nanocatalysts for hydrogenative transformations.

#### Acknowledgements

This work was financially supported by the Chinese Academy of Sciences, the National Natural Science Foundation of China (21373246, 21522309 and 21503242) and Suzhou Science and Technology Projects (SYG201518 and SYG201519) for generous financial support.

#### Appendix A. Supplementary data

Supplementary data associated with this article can be found, in the online version, at <http://dx.doi.org/10.1016/j.apcatb.2016.10.038>.

#### References

- [1] D.M. Alonso, S.G. Wettstein, J.A. Dumesic, *Chem. Soc. Rev.* 41 (2012) 8075–8098.
- [2] X. Kong, R.X. Zheng, Y.F. Zhu, G.Q. Ding, Y.L. Zhu, Y.W. Li, *Green Chem.* 17 (2015) 2504–2514.

[3] K. Yan, Y.Y. Yang, J.J. Chai, Y.R. Lu, *Appl. Catal. B: Environ.* 179 (2015) 292–304.

[4] M. Sankar, N. Dimitratos, P.J. Miedziak, P.P. Wells, C.J. Kiely, G.J. Hutchings, *Chem. Soc. Rev.* 41 (2012) 8099–8139.

[5] M.J. Taylor, I.J. Durndell, M.A. Isaacs, C.M. Parlett, K. Wilson, A.F. Lee, G. Kyriakou, *Appl. Catal. B: Environ.* 180 (2016) 580–585.

[6] N.S. Biradar, A.M. Hengne, S.N. Birajdar, P.S. Niphadkar, P.N. Joshi, C.V. Rode, *ACS Sustain. Chem. Eng.* 2 (2014) 272–281.

[7] S. Sitthisa, W. An, D.E. Resasco, *J. Catal.* 284 (2011) 90–101.

[8] Y. Shi, Y.L. Zhu, Y. Yang, Y.W. Li, H.J. Jiao, *ACS Catal.* 5 (2015) 4020–4032.

[9] Y.L. Yang, Z.T. Du, Y.Z. Huang, F. Lu, F. Wang, J. Gao, J. Xu, *Green Chem.* 15 (2013) 1932–1940.

[10] X.L. Li, J. Deng, J. Shi, T. Pan, C.G. Yu, H.J. Xu, Y. Fu, *Green Chem.* 17 (2015) 1038–1046.

[11] T. Mizugaki, T. Yamakawa, Y. Nagatsu, Z. Maeno, T. Mitsudome, K. Jitsukawa, K. Kaneda, *ACS Sustain. Chem. Eng.* 2 (2014) 2243–2247.

[12] S. Koso, N. Ueda, Y. Shinmi, K. Okumura, T. Kizuka, K. Tomishige, *J. Catal.* 267 (2009) 89–92.

[13] R. Mariscal, P. Maireles-Torres, M. Ojeda, I. Sadaba, M. López Granados, *Energy Environ. Sci.* 9 (2016) 1144–1189.

[14] H. Adkins, R. Connor, *J. Am. Chem. Soc.* 53 (1931) 1091–1095.

[15] M.M. Villaverde, N.M. Bertero, T.F. Garetto, A.J. Marchi, *Catal. Today* 213 (2013) 87–92.

[16] K. Yan, J.Y. Liao, X. Wu, X.M. Xie, *RSC Adv.* 3 (2013) 3853–3856.

[17] Q.Q. Yuan, D.M. Zhang, L. van Haandel, F.Y. Ye, T. Xue, E.J. Hensen, Y.J. Guan, *J. Mol. Catal. A: Chem.* 406 (2015) 58–64.

[18] J.Z. Chen, F. Lu, J.J. Zhang, W.Q. Yu, F. Wang, J. Gao, J. Xu, *ChemCatChem* 5 (2013) 2822–2826.

[19] K. Yan, C. Jarvis, T. Lafleur, Y.X. Qiao, X.M. Xie, *RSC Adv.* 3 (2013) 25865–25871.

[20] J. Lee, Y.T. Kim, G.W. Huber, *Green Chem.* 16 (2014) 708–718.

[21] T.P. Sulmonetti, S.H. Pang, M.T. Cloure, S. Lee, D.A. Cullen, P.K. Agrawal, C.W. Jones, *Appl. Catal. A: Gen.* 517 (2016) 187–195.

[22] C.M. Li, Y.D. Chen, S.T. Zhang, S.M. Xu, J.Y. Zhou, F. Wang, M. Wei, D.G. Evans, X. Duan, *Chem. Mater.* 25 (2013) 3888–3896.

[23] R.V. Maligal-Ganesh, C.X. Xiao, T.W. Goh, L.L. Wang, J. Gustafson, Y.C. Pei, Z.Y. Q, D.D. Johnson, S.R. Zhang, F. (Feng) Tao, W.Y. Huang, *ACS Catal.* 6 (2016) 1754–1763.

[24] M.A. Tike, V.V. Mahajani, *Ind. Eng. Chem. Res.* 46 (2007) 3275–3282.

[25] F.A. Khan, A. Vallat, G. Stüss-Fink, *Catal. Commun.* 12 (2011) 1428–1431.

[26] B. Zhang, Y.L. Zhu, G.Q. Ding, H.Y. Zheng, Y.W. Li, *Green Chem.* 14 (2012) 3402–3409.

[27] Y. Nakagawa, K. Tomishige, *Catal. Commun.* 12 (2010) 154–156.

[28] B.F. Chen, F.B. Li, Z.J. Huang, G.Q. Yuan, *Appl. Catal. A: Gen.* 500 (2015) 23–29.

[29] Q.Q. Yuan, F.Y. Ye, T. Xue, Y.J. Guan, *Appl. Catal. A: Gen.* 507 (2015) 26–33.

[30] Y. Nakagawa, K. Takada, M. Tamura, K. Tomishige, *ACS Catal.* 4 (2014) 2718–2726.

[31] X.C. Chen, W. Sun, N. Xiao, Y.J. Yan, S.W. Liu, *Chem. Eng. J.* 126 (2007) 5–11.

[32] N. Merat, C. Godawa, A. Gaset, *J. Chem. Technol. Biotechnol.* 48 (1990) 145–159.

[33] F. Studt, F. Abild-Pedersen, Q.X. Wu, A.D. Jensen, B. Temel, J.-D. Grunwaldt, J.K. Nørskov, *J. Catal.* 293 (2012) 51–60.

[34] L.-C. Chen, S.D. Lin, *Appl. Catal. B: Environ.* 106 (2011) 639–649.

[35] L. De Rogatis, T. Montini, A. Cognigni, L. Olivi, P. Fornasiero, *Catal. Today* 145 (2009) 176–185.

[36] A. Ungureanu, B. Dragoi, A. Chiriac, C. Ciotonea, S. Royer, D. Duprez, A.S. Mamede, E. Dumitriu, *ACS Appl. Mater. Interfaces* 5 (2013) 3010–3025.

[37] S.H. Pang, N.E. Love, J.W. Medlin, *J. Phys. Chem. Lett.* 5 (2014) 4110–4114.

[38] K. Mori, K. Miyawaki, H. Yamashita, *ACS Catal.* 6 (2016) 3128–3135.

[39] R.L. Manfro, T.P. Pires, N.F. Ribeiro, M.M. Souza, *Catal. Sci. Technol.* 3 (2013) 1278–1287.

[40] D.L. Li, M.M. Lu, K. Aragaki, M. Koike, Y. Nakagawa, K. Tomishige, *Appl. Catal. B: Environ.* 192 (2016) 171–181.

[41] A.R. Naghash, T.H. Etsell, S. Xu, *Chem. Mater.* 18 (2006) 2480–2488.

[42] J. Ahmed, K.V. Ramanujachary, S.E. Lofland, A. Furiato, G. Gupta, S.M. Shivaprasad, A.K. Ganguli, *Colloids Surf. A* 331 (2008) 206–212.

[43] A. Ungureanu, B. Dragoi, A. Chiriac, S. Royer, D. Duprez, E. Dumitriu, *J. Mater. Chem.* 21 (2011) 12529–12541.

[44] Q.X. Wu, L.D. Duchstein, G.L. Chiarello, J.M. Christensen, C.D. Damsgaard, C.F. Elkjaer, J.B. Wagner, B. Temel, J.-D. Grunwaldt, A.D. Jensen, *ChemCatChem* 6 (2014) 301–310.

[45] C.M. Li, J.Y. Zhou, W. Gao, J.W. Zhao, J. Liu, Y.F. Zhao, M. Wei, D.G. Evans, X. Duan, *J. Mater. Chem. A* 1 (2013) 5370–5376.

[46] Y.F. Zhao, B. Zhao, J.J. Liu, G.B. Chen, R. Gao, S.Y. Yao, M.Z. Li, Q.H. Zhang, L. Gu, J.L. Xie, X.D. Wen, L.-Z. Wu, C.-H. Tung, D. Ma, T.R. Zhang, *Angew. Chem. Int. Ed.* 55 (2016) 4215–4219.

[47] S.J. Park, H.A. Ahn, I.J. Heo, I.-S. Nam, J.H. Lee, Y.K. Youn, H.J. Kim, *Top. Catal.* 53 (2010) 57–63.

[48] Y. Yang, G. Gao, X. Zhang, F.W. Li, *ACS Catal.* 4 (2014) 1419–1425.

[49] Z.L. Li, J.H. Liu, Z.W. Huang, Y. Yang, C.G. Xia, F.W. Li, *ACS Catal.* 3 (2013) 839–845.

[50] Z.L. Li, G.L. Li, L.H. Jiang, J.L. Li, G.Q. Sun, C.G. Xia, F.W. Li, *Angew. Chem. Int. Ed.* 54 (2015) 1494–1498.

[51] A.I. Tsyganok, T. Tsunoda, S. Hamakawa, K. Suzuki, K. Takehira, T. Hayakawa, *J. Catal.* 213 (2003) 191–203.

[52] D.L. Li, L. Wang, M. Koike, Y. Nakagawa, K. Tomishige, *Appl. Catal. B: Environ.* 102 (2011) 528–538.

[53] V. Rives, M.A. Ulibarri, A. Montero, *Appl. Clay Sci.* 10 (1995) 83–93.

[54] E.T. Saw, U. Oemar, X.R. Tan, Y. Du, A. Borgna, K. Hidajat, S. Kawi, *J. Catal.* 314 (2014) 32–46.

[55] S. Sitthisa, D.E. Resasco, *Catal. Lett.* 141 (2011) 784–791.

[56] H. Yen, Y. Seo, S. Kalilaguine, F. Kleitz, *ACS Catal.* 5 (2015) 5505–5511.

[57] Y.F. Zhu, X. Kong, X.Q. Li, G.Q. Ding, Y.L. Zhu, Y.W. Li, *ACS Catal.* 4 (2014) 3612–3620.

[58] W.J. Xu, H.F. Wang, X.H. Liu, J.W. Ren, Y.Q. Wang, G.Z. Lu, *Chem. Commun.* 47 (2011) 3924–3926.

[59] D. Al-Mawlawi, J.M. Saleh, *J. Chem. Soc. Faraday Trans. I* 77 (1981) 2965–2976.

[60] X.Y. Wang, R. Rinaldi, *ChemSusChem* 5 (2012) 1455–1466.

[61] I. McManus, H. Daly, J.M. Thompson, E. Connor, C. Hardacre, S.K. Wilkinson, N. Sedaie Bonab, J. ten. Dam, M.J.H. Simmons, E.H. Stitt, C. D'Agostino, J. McGregor, L.F. Gladden, J.J. Delgado, *J. Catal.* 330 (2015) 344–353.